Hindawi
Complexity
Volume 2020, Article ID 5875191, 15 pages
https://doi.org/10.1155/2020/5875191

Research Article

Nonsingular Fast Terminal Adaptive Neuro-sliding Mode Control for Spacecraft Formation Flying Systems

Xiaohan Lin,[1] **Xiaoping Shi**,[1] **Shilun Li**,[2] **Sing Kiong Nguang**,[3] **and Liruo Zhang**[3]

[1]*Control and Simulation Center, Harbin Institute of Technology, Harbin 150080, China*
[2]*School of Astronautics, Harbin Institute of Technology, Harbin 150001, China*
[3]*Department of Electrical, Computer and Software Engineering, The University of Auckland, Auckland 1142, New Zealand*

Correspondence should be addressed to Xiaohan Lin; hitlinxh@hotmail.com

Received 9 March 2020; Revised 23 April 2020; Accepted 11 May 2020; Published 30 May 2020

Academic Editor: Xianming Zhang

In this paper, a nonsingular fast terminal adaptive neurosliding mode control for spacecraft formation flying systems is investigated. First, a supertwisting disturbance observer is employed to estimate external disturbances in the system. Second, a fast nonsingular terminal sliding mode control law is proposed to guarantee the tracking errors of the spacecraft formation converge to zero in finite time. Third, for the unknown parts in the spacecraft formation flying dynamics, we proposed an adaptive neurosliding mode control law to compensate them. The proposed sliding mode control laws not only achieve the formation but also alleviate the effect of the chattering. Finally, simulations are used to demonstrate the effectiveness of the proposed control laws.

1. Introduction

With the increasing applications of the spacecraft formation flying system, the importance of improving system performance of complicated spacecraft with practical control design has gained much attention over recent years [1–5]. In the spacecraft formation flying system, stability is the most essential problem to be solved [6]. Many control methods have been applied to solve these problems in the literature, such as the adaptive control [7], sliding mode control [8], backstepping technique control [9], fuzzy control [10], optimal control [11], and H_∞ control [12]. However, along with the goal of stabilization for the spacecraft, the disturbances and uncertainties should also be considered, which is often neglected in some research [13].

Sliding mode control is widely used due to its advantages of robustness against external disturbances [14–16] and parameter uncertainties [17], especially in spacecraft formation flying system. In sliding mode control, chattering is a common phenomenon that often degrades system performance and even causes instability. To deal with this problem, the terminal sliding mode control is developed, in which some nonlinear terms are introduced in the sliding surface. In [18], the case of spacecraft final approach, combining with the continuously differential collision avoidance state constraint function is studied and an improved terminal sliding surface is presented. In [19], based on the conditions of external disturbances and inertial uncertain parameters, Ran et al. have proposed the adaptive fuzzy terminal sliding mode control for the second-order spacecraft attitude manoeuvre system and the convergence time of the sliding surface has been reduced. In [20], a new nonsingular terminal sliding mode (NTSM) surface has been introduced to eliminate singularity within the finite time. An adaptive nonsingular terminal sliding mode control also has been presented for an attitude tracking of spacecraft with actuator faults to avoid singularity [21]. Although several drawbacks of the sliding mode control have been compensated by the modified control laws, due to the high-frequency reaching control term in the control input [22], the chattering problem still needs to be solved. In [23], a fractional order control law based on the nonsingular terminal supertwisting sliding mode control is proposed to achieve system stability and accurately estimate the unknown model. Consequently,

the nonsingular fast terminal sliding mode surface has the ability to reduce the chattering and solve the singularity problem.

In practical spacecraft formation flying systems, internal and external disturbances are inevitable. Many control methods have been used to solve this problem [24, 25]. The disturbance observers have been widely considered to estimate the disturbances [26]. In [27], an extended state observer is introduced to estimate disturbances for the multiagent systems with unknown nonlinear dynamics and disturbances. Furthermore, by simultaneously taking the output measurement and delayed control input into account, the extended observer has been used to estimate the unmeasurable system states and the additive disturbances [28]. To have a smaller estimation error of the disturbance, high-order disturbance observers have been investigated in [29]. Among all types of high-order observer, the supertwisting disturbance observer stands out due to its ability of avoiding the excessively high order observer gains that can cause sensor noise within fixed bandwidth [30].

Despite the external disturbances, uncertainties in practical formation flying systems are also inevitable; however, their impacts on the system's performance have not been studied in most of the aforementioned results. In practice, parameter uncertainties may have direct impact on system performance [31]; hence, it is critical to deal with the problem of uncertainties. Due to the advantage of the neural networks in approximating nonlinear functions, it can be applied in dealing with the nonlinearity in the spacecraft formation systems as well [32–34]. Based on neural network and backstepping techniques, a distributed adaptive coordinated control algorithm has been proposed in [35], which effectively solves the chattering problem. To achieve robustness, in [36], a robust adaptive fuzzy PID-type sliding mode control has been designed with the neural network, with which the system stability is ensured and the transient performance is improved. In [37], the global adaptive neural control for a general class of nonlinear robot manipulators has been proposed, in which the transient performance and robustness are both improved. Compared with other neural networks [38–40], the Radial Basis Function (RBF) neural network stands out given its strong robustness and excellent performance of nonlinear approximation [41]. Therefore, it is desirable to use the RBF neural network to estimate and compensate for the nonlinear functions in the spacecraft formation flying system.

Motivated by the above observations, in this paper, a novel nonsingular fast terminal adaptive neurosliding mode control for the spacecraft formation flying system is proposed. The proposed control law guarantees that the tracking errors converge to zero in finite time. By using an adaptive RBF neural network, the uncertainties in the spacecraft formation flying system is compensated. The contributions of the paper can be summarized as follows:

(1) External disturbances are estimated by a supertwisting disturbance observer in finite time. The supertwisting disturbance observer can avoid high observer gains that may amplify the noises of the sensors.

(2) Compared with [42], our novel fast nonsingular terminal sliding mode control law achieves the stability of spacecraft formation flying system within finite time. Moreover, the singularity is avoided and the chattering problem is also alleviated.

(3) If some of the nonlinear dynamics in the spacecraft formation system are unknown, an adaptive RBF neural network control law is proposed to approximate those nonlinear dynamics.

The remaining parts of the paper are arranged as follows. The background of the spacecraft formation flying system is introduced in Section 2. In Section 3, the proposed control laws and stability analysis are presented. Simulation results are given to verify the effectiveness of the proposed control laws in Section 4. Finally, some conclusions are given in Section 5.

1.1. Notations. The following notations are used throughout this paper. For a vector $x = [x_1, x_2, \ldots, x_n]^{\mathrm{T}} \in \mathbb{R}^n$ and $|x|_d \triangleq \mathrm{diag}\{|x_1|, |x_2|, \ldots, |x_n|\}$, the standard sign function is defined as $\mathrm{sign}(x) = [\mathrm{sign}(x_1), \mathrm{sign}(x_2), \ldots, \mathrm{sign}(x_n)]^{\mathrm{T}}$. The Euclidean norm of vector x is denoted as $\|x\| = \sqrt{x^{\mathrm{T}}x}$. For a matrix $A \in \mathbb{R}^{n\times n}$, $\|A\|_1$ denotes the maximum absolute column sum norm. $\|A\|_2 = \sqrt{\lambda_{\max}(A^{\mathrm{T}}A)}$ is the 2-norm, where $\lambda_{\max}$ means the maximum eigenvalue. $\mathrm{tr}(A)$ denotes the trace of A. $I_{n\times n}$ denotes $n \times n$ identity matrix. For a three-dimensional vector $x = [x_1, x_2, x_3]^{\mathrm{T}}$, the skew-symmetric matrix $x^{\times} \in \mathbb{R}^{3\times 3}$ is defined as follows:

$$x^{\times} = \begin{bmatrix} 0 & -x_3 & x_2 \\ x_3 & 0 & -x_1 \\ -x_2 & x_1 & 0 \end{bmatrix}. \tag{1}$$

2. Spacecraft Formation Systems and Preliminaries

In this section, the spacecraft formation flying system and some useful lemmas are presented.

2.1. Spacecraft Formation Flying System. The relative orbit motion under the chaser spacecraft coordinate frame is shown in Figure 1. F_I denotes the equatorial inertial coordinate frame $(O_I X_I Y_I Z_I)$, F_t is located at the centroid of the target spacecraft, and the coordinate axis of the target spacecraft coincides with the main inertia axis F_I, the x_t-axis points to the solar panel, the y_t-axis is perpendicular to the longitudinal plane of x_t-axis, and z_t-axis satisfies the rule of the right hand. The chaser spacecraft coordinate frame F_c is similar to the coordinate frame F_t.

Assume that the active control force of the target spacecraft is zero, and the dynamic models of the target spacecraft and the chaser spacecraft are given as follows:

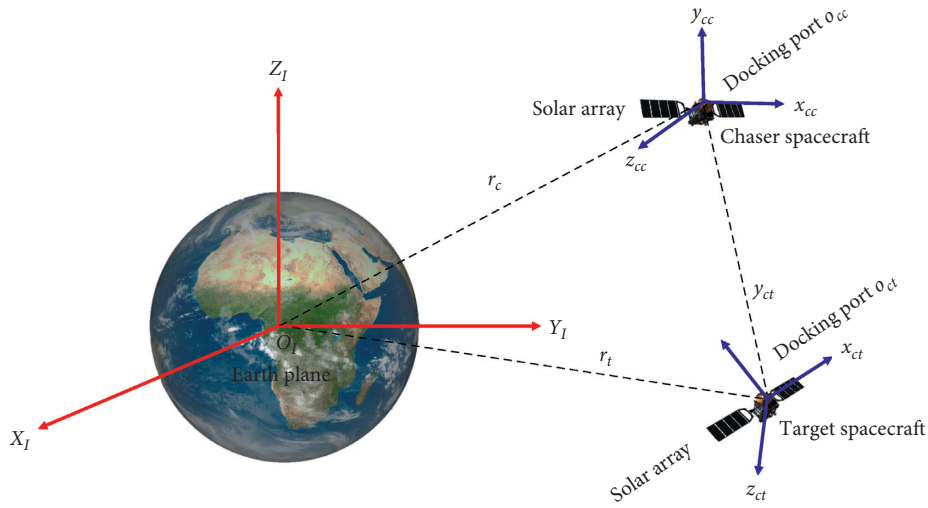

Figure 1: The relative orbit motion model of the spacecraft formation flying system.

$$\ddot{r}_t = -\frac{\mu_e}{r_t^3} r_t + \frac{d_{ct}}{m_t}, \tag{2}$$

$$\ddot{r}_c = -\frac{\mu_e}{r_c^3} r_c + \frac{d_{cc}}{m_c} + \frac{f_{cc}}{m_c}, \tag{3}$$

where m_t and m_c denote the masses of the target spacecraft and the chaser spacecraft and $d_{ct} \in \mathbb{R}^3$ and $d_{cc} \in \mathbb{R}^3$ denote the external perturbation forces of the target spacecraft and the chaser spacecraft, respectively. $f_{cc} \in \mathbb{R}^3$ is the control force of the chaser spacecraft. $r_t = \|r_t\|_2$ and $r_c = \|r_c\|_2$, where r_t and r_c denote the position vectors of the target spacecraft and chaser spacecraft to the geocentric, respectively.

Define $\rho = r_c - r_t$; then, from (2) and (3) the relative acceleration vector is obtained as

$$\ddot{\rho} = -\frac{\mu_e}{r_c^3} r_c + \frac{\mu_e}{r_t^3} r_t + \frac{d_{cc}}{m_c} - \frac{d_{ct}}{m_t} + \frac{f_{cc}}{m_c}. \tag{4}$$

Furthermore, let ρ_c denote the projection vector in the chaser spacecraft body coordinate frame F_c, which denotes

$$\begin{aligned} f_c &= -\frac{\mu_e}{r_c^3} r_c + \frac{\mu_e}{r_t^3} r_t, \\ d_c &= d_{cc} - \frac{m_c d_{ct}}{m_t}, \\ u_c &= f_{cc}. \end{aligned} \tag{5}$$

Then,

$$\ddot{\rho}_c + \omega_c^{\times}\left(\omega_c^{\times}\rho_c\right) + 2\omega_c^{\times}\dot{\rho}_c + \dot{\omega}_c^{\times}\rho_c = f_c + \frac{d_c}{m_c} + \frac{u_c}{m_c}, \tag{6}$$

where $\omega_c = [\omega_{c1}, \omega_{c2}, \omega_{c3}]^{\mathrm{T}}$ is the angular velocity of F_c relative to the inertial coordinate frame F_I under F_c frame.

In this paper, the desired relative position and velocity under F_c frame are assumed to be ρ_{cd} and 0, respectively. Then, the error vector can be expressed as $e_c = \rho_c - \rho_{cd}$; then, (6) can be written as the Euler–Lagrange equation form to express the orbit relative motion:

$$m_c\ddot{e}_c + A_c\dot{e}_c + B_c e_c + g_c = u_c + d_c, \tag{7}$$

where

$$\begin{aligned} A_c &= 2m_c\omega_c^{\times}, \\ B_c &= m_c\begin{bmatrix} -\omega_{c2}^2 - \omega_{c3}^2 & \omega_{c1}\omega_{c2} - \dot{\omega}_{c3} & \omega_{c1}\omega_{c3} + \dot{\omega}_{c2} \\ \omega_{c1}\omega_{c2} + \dot{\omega}_{c3} & -\omega_{c1}^2 - \omega_{c3}^2 & \omega_{c2}\omega_{c3} - \dot{\omega}_{c1} \\ \omega_{c1}\omega_{c3} - \dot{\omega}_{c2} & \omega_{c2}\omega_{c3} + \dot{\omega}_{c1} & -\omega_{c1}^2 - \omega_{c2}^2 \end{bmatrix}, \\ g_c &= -m_c f_c + m_c\ddot{r}_{dc} + A_c\dot{r}_{dc} + B_c r_{dc}. \end{aligned} \tag{8}$$

The Modified Rodrigues Parameters (MRPs) are used to describe the attitude dynamics of the chaser spacecraft which can be defined as

$$\sigma = \frac{\widehat{q}}{1 + \overline{q}} = k_e \tan\frac{\varphi}{4}, \tag{9}$$

where $q = [\overline{q}, \widehat{q}^{\mathrm{T}}]^{\mathrm{T}}$ denotes attitude quaternion and k_e and $\varphi \in (-2\pi, 2\pi)$ denote Euler axis and Euler angular of the attitude rotation, respectively.

Then, the attitude kinematics and the dynamics of the chaser spacecraft are given as

$$\begin{aligned} \dot{\sigma} &= G(\sigma)\omega_c, \\ G(\sigma) &= \frac{1}{4}\left[\left(1 - \sigma^T\sigma\right)I_{3\times 3} + 2\sigma^{\times} + 2\sigma\sigma^T\right], \\ J\dot{\omega}_c &= -\omega_c^{\times}J\omega_c + u_\tau + d_\tau, \end{aligned} \tag{10}$$

where $J \in \mathbb{R}^{3\times 3}$ denotes the inertia matrix of the chaser spacecraft and $u_\tau \in \mathbb{R}^3$ and $d_\tau \in \mathbb{R}^3$ denote the control torque and the external disturbance torque of the chaser spacecraft, respectively.

Defining the error attitude σ_e and the error angular velocity ω_e as

$$\sigma_e = \frac{(1-\sigma_d^{\mathrm{T}}\sigma_d)\sigma - (1-\sigma^{\mathrm{T}}\sigma)\sigma_d + 2\sigma^{\times}\sigma_d}{1+\sigma^{\mathrm{T}}\sigma\sigma_d^{\mathrm{T}}\sigma_d + 2\sigma_d^{\mathrm{T}}\sigma},$$

$$\omega_e = \omega_c - R(\sigma_e)\omega_d, \tag{11}$$

$$R(\sigma) = I_{3\times3} - \frac{4(1-\sigma^{\mathrm{T}}\sigma)}{(1+\sigma^{\mathrm{T}}\sigma)^2}\sigma^{\times} + \frac{8\sigma^{\times}}{(1+\sigma^{\mathrm{T}}\sigma)^2}\sigma^{\times},$$

where $\sigma_d \in \mathbb{R}^3$ denotes the desired attitude and $\omega_d \in \mathbb{R}^3$ denotes the desired angular velocity. Furthermore, the attitude model of the chaser spacecraft can be expressed as the Euler–Lagrange form:

$$M_\tau \ddot{\sigma}_e + A_\tau \dot{\sigma}_e + g_\tau = G^{-\mathrm{T}}(\sigma_e)d_\tau + G^{-\mathrm{T}}(\sigma_e)u_\tau, \tag{12}$$

where

$$\begin{aligned}
M_\tau &= G^{-\mathrm{T}}(\sigma_e)JG^{-1}(\sigma_e),\\
G(\sigma_e) &= \frac{1}{4}\left[\left(1-\sigma_e^{\mathrm{T}}\sigma_e\right)I_{3\times3} + 2\sigma_e^{\times} + 2\sigma_e\sigma_e^{\mathrm{T}}\right],\\
A_\tau &= -G^{-\mathrm{T}}(\sigma_e)\left[\left(JG^{-1}(\sigma_e)\dot{\sigma}_e\right)^{\times}G^{-1}(\sigma_e) + J\dot{G}^{-1}(\sigma_e)\right]\\
&\quad + G^{-\mathrm{T}}(\sigma_e)\left[J\left(R(\sigma_e)\omega_d\right)^{\times} + \left(R(\sigma_e)\omega_d\right)^{\times}J\right.\\
&\quad \left. - \left(JR(\sigma_e)\omega_d\right)^{\times}\right]G^{-1}(\sigma_e),\\
g_\tau &= G^{-\mathrm{T}}(\sigma_e)\left(\left(R(\sigma_e)\omega_d\right)^{\times}JR(\sigma_e)\omega_d + JR(\sigma_e)\dot{\omega}_d\right).
\end{aligned} \tag{13}$$

In order to describe the attitude-orbit coupling dynamics motion of the spacecraft formation uniformly, define

$$x_e = \begin{bmatrix} \sigma_e \\ e_c \end{bmatrix}, \quad u = \begin{bmatrix} u_\tau \\ u_c \end{bmatrix}, \quad d = \begin{bmatrix} d_\tau \\ d_c \end{bmatrix}. \tag{14}$$

Then, based on (5) and (22), the attitude-orbit coupling model is given as

$$\dot{x}_e = x_{de}, \tag{15}$$

$$M\dot{x}_{de} = -Ax_{de} - g + C_1u + C_2d, \tag{16}$$

where

$$M = \begin{bmatrix} M_\tau & \mathbf{0}_{3\times3} \\ \mathbf{0}_{3\times3} & m_cI_{3\times3} \end{bmatrix}, \tag{17}$$

$$A = \begin{bmatrix} A_\tau & \mathbf{0}_{3\times3} \\ \mathbf{0}_{3\times3} & A_c \end{bmatrix}, \tag{18}$$

$$g = \begin{bmatrix} g_\tau \\ B_ce_c + g_c \end{bmatrix}, \tag{19}$$

$$C_1 = C_2 = \begin{bmatrix} G^{-\mathrm{T}}(\sigma_e) & 0_{3\times3} \\ 0_{3\times3} & I_{3\times3} \end{bmatrix}. \tag{20}$$

Remark 1. It can be seen in (12), the attitude and orbit in the spacecraft formation flying system are coupled. Therefore, it is necessary to build the spacecraft coupling motion model (15) and (16) to enhance the control accuracy and efficiency. From (15) and (16), it can be seen that the coupling of attitude and orbit is reflected by the matrix B_c and the vector d_τ simultaneously. B_c represents the attitude effect on orbit. In addition, the gravity gradient torque contains orbit information, and the disturbance torque can reflect the influence of the orbit on the attitude, thus d_τ can reflect the influence of the orbit on the attitude.

Assumption 1. The external disturbance vector $d = [d_1, \ldots, d_6]$ in the spacecraft formation flying system (15) and (16) is assumed to satisfy $\|d\| \le d_m$ and $|\dot{d}_i| \le \varsigma_i$, where $d_m > 0$ and $\varsigma_i > 0$.

Assumption 2. All the state variables of the spacecraft formation flying system are assumed to be measurable.

2.2. Preliminary Knowledge. In this section, some related lemmas and definitions in this paper are given below.

Lemma 1 (see [43]). *For $\dot{x} = f(x,t)$, $f(0,t) = 0$ and $x \in U_0 \subset R^n$, where $f: U_0 \times R^+ \longrightarrow R^n$ is continuous with respect to x on an open neighborhood U_0 of the origin $x = 0$. Suppose that there are a positive-definite function $V(x,t)$ (defined on $\widehat{U} \times R^+$, where $\widehat{U} \in U_0 \in R^n$ is a neighborhood of the origin), real numbers $c > 0$ and $0 < \alpha < 1$, such that $\dot{V}(x,t) + cV^{\alpha}(x,t)$ is negative semidefinite on $\widehat{U}$. Then, $V(x,t)$ is locally finite-time convergent, or equivalently, and becomes 0 locally in finite time, with its setting time $T \le V(x(t_0),t_0)^{1-\alpha}/c(1-\alpha)$ for a given initial condition $x(t_0)$ in a neighborhood of the origin in $\widehat{U}$.*

Lemma 2 (see [44]). *Suppose Lyapunov function $V(\widehat{z})$ is defined on a neighborhood $U \subset R^n$ of the origin, and $\dot{V}(\widehat{z}) + \lambda_0V^{\ell} \le 0$ in which $\lambda_0 > 0$, $0 < \ell < 1$. Then, there exists an area $U_0 \subset R^n$ such that any $V(\widehat{z})$ that start from $U_0 \subset R^n$ can reach $V(\widehat{z}) \equiv 0$ within finite time $T_f \le V^{1-\ell}(0)/\lambda_0(1-\ell)$ in which $V(0)$ is the initial time of $V(\widehat{z})$.*

Definition 1 (see [45]). For the autonomous system,

$$\dot{\widehat{z}} = f(\widehat{z}), \tag{21}$$

where $\widehat{z} \in R^N$ and $f(0) = 0$, if the Lyapunov function $V(\widehat{z})$ satisfies the following conditions:

(a) $V(\widehat{z})$ is a positive continuous differentiable function

(b) There exist $\alpha_1 > 0$, $\alpha_2 > 0$, $p \in (0,1)$, and an open neighborhood $U \subset U_0$ containing the origin, such that the inequality $\dot{V}(\widehat{z}) \le -\alpha_1V(\widehat{z}) - \alpha V^p(\widehat{z})$ holds; then, it can be concluded that the origin is the finite time stable equilibrium of system (20)

3. Control Law Design

In this section, first, we employ a supertwisting observer to estimate the external disturbances in the system. Second, we propose a fast nonsingular terminal sliding mode control law along with the supertwisting disturbance observer for the spacecraft formation flying system. In the last section, the nonlinear matrices A and g in (18) and (19), respectively, are assumed to be unknown, and an adaptive neurosliding model control law for the spacecraft formation flying system is proposed.

3.1. The Fast Nonsingular Terminal Sliding Mode Control Law with a Supertwisting Disturbance Observer. The block diagram of the fast nonsingular terminal sliding mode control law with the supertwisting disturbance observer is shown in Figure 2. In Figure 2, it can be seen that the overall control law consists of two parts: a fast nonsingular terminal sliding mode control law along with the supertwisting disturbance observer. The supertwisting disturbance observer is applied to estimate the disturbances for the spacecraft formation flying system if the system dynamics are known.

3.1.1. Supertwisting Disturbance Observer. In practical applications, the disturbances in the spacecraft formation flying system are fast time-varying disturbances. Hence, it is difficult for conventional observers to estimate those disturbances. In this section, a supertwisting disturbance observer is employed to estimate those disturbances. The supertwisting disturbance observer can estimate the disturbance in finite time and also it avoids high-order observer gains with fixed bandwidth.

According to the attitude-orbit coupling system (15) and (16), the disturbance vector d can be rewritten as follows:

$$d = C_2^{-1}\left(M\ddot{x}_e + A\dot{x}_e + g - C_1 u\right). \tag{22}$$

Define the state variables as follows:

$$\begin{aligned} x_1 &= \int_0^t d\mathrm{d}t \\ &= C_2^{-1}M\dot{x}_e - \int_0^t \frac{\mathrm{d}}{\mathrm{d}t}\left(C_2^{-1}M\right)\dot{x}_e + C_2^{-1}\left(A\dot{x}_e + g - C_1 u\right)\mathrm{d}t, \\ x_2 &= d. \end{aligned} \tag{23}$$

Then, the disturbance dynamic system for the spacecraft formation flying is given as

$$\begin{aligned} \dot{x}_1 &= x_2, \\ \dot{x}_2 &= \dot{d}. \end{aligned} \tag{24}$$

For each disturbance d_i in the spacecraft formation flying system, the disturbance's model is given as follows:

$$\begin{aligned} \dot{x}_{1i} &= x_{2i}, \\ \dot{x}_{2i} &= \dot{d}_i, \quad i = 1, 2, \ldots, 6. \end{aligned} \tag{25}$$

The supertwisting disturbance observer is given as follows:

$$\begin{aligned} \dot{\widetilde{x}}_{1i} &= -\lambda_1 \left|e_{1i}\right|^{1/2}\mathrm{sign}\left(e_{1i}\right) + \widetilde{x}_{2i}, \\ \dot{\widetilde{x}}_{2i} &= -\lambda_2 \mathrm{sign}\left(e_{1i}\right), \end{aligned} \tag{26}$$

where λ_1 and λ_2 denote the positive observer gains, $\widetilde{x}_{1i}$ and $\widetilde{x}_{2i}$ are the estimations of the state vectors x_{1i} and x_{2i}, and $e_{1i} = \widetilde{x}_{1i} - x_{1i}$ and $e_{2i} = \widetilde{x}_{2i} - x_{2i}$ are the estimation errors, respectively.

According to the attitude-orbit coupling system (15) and (16) and the supertwisting state observer (26), the estimation errors can be rewritten as

$$\begin{aligned} \dot{e}_{1i} &= -\lambda_1 \left|e_{1i}\right|^{1/2}\mathrm{sign}\left(e_{1i}\right) + e_{2i}, \\ \dot{e}_{2i} &= -\lambda_2 \mathrm{sign}\left(e_{1i}\right) - \dot{d}_i. \end{aligned} \tag{27}$$

Define the state vectors $\kappa = [\kappa_1, \kappa_2]^{\mathrm{T}}$, where $\kappa_1 = |e_{1i}|^{1/2}\mathrm{sign}\left(e_{1i}\right)$, $\kappa_2 = e_{2i}$.

Then, the derivatives of the state vectors κ_1 and κ_2 can be written as

$$\begin{aligned} \dot{\kappa}_1 &= -\frac{\lambda_1}{2}\left|e_{1i}\right|^{-1}e_{1i} + \frac{1}{2}\left|e_{1i}\right|^{-(1/2)}e_{2i}, \\ \dot{\kappa}_2 &= -\lambda_2\left|e_{1i}\right|^{-1}e_{1i} - \dot{d}_i. \end{aligned} \tag{28}$$

Similar to [46], the following Lyapunov function for (28) is constructed:

$$\begin{aligned} V_{st} &= \kappa^{\mathrm{T}}\theta_1\kappa \\ &= \frac{1}{2}\left(\lambda_1^2 + 4\lambda_2\right)\kappa_1^2 - \lambda_1\kappa_1\kappa_2 + \kappa_2^2, \end{aligned} \tag{29}$$

where $\theta_1 = 1/2\begin{bmatrix} \left(\lambda_1^2 + 4\lambda_2\right) & -\lambda_1 \\ -\lambda_1 & 2 \end{bmatrix}$.

Then, the derivative of Lyapunov function V_{st} with respect to the time is given as

$$\begin{aligned} \dot{V}_{st} &= \left(\lambda_1^2 + 4\lambda_2\right)\kappa_1\dot{\kappa}_1 - \lambda_1\dot{\kappa}_1\kappa_2 - \lambda_1\kappa_1\dot{\kappa}_2 + 2\kappa_2\dot{\kappa}_2 \\ &= \left(\lambda_1^2 + 4\lambda_2\right)\left|e_{1i}\right|^{-(1/2)}e_{1i}\left(-\frac{\lambda_1}{2}\left|e_{1i}\right|^{-1}e_{1i} + \frac{1}{2}\left|e_{1i}\right|^{-(1/2)}e_{2i}\right) \\ &\quad + \frac{\lambda_1^2}{2}\left|e_{1i}\right|^{-1}e_{1i}e_{2i} - \frac{\lambda_1}{2}\left|e_{1i}\right|^{-(1/2)}e_{2i}^2 \\ &\quad - \lambda_1\left|e_{1i}\right|^{-(1/2)}e_{1i}\left(-\lambda_2\left|e_{1i}\right|^{-1}e_{1i} - \dot{d}_i\right) \\ &\quad - 2\lambda_2\left|e_{1i}\right|^{-1}e_{1i}e_{2i} - 2e_{2i}\dot{d}_i \\ &= \left(\lambda_1^2 + 4\lambda_2\right)\left(-\frac{\lambda_1}{2}\left|e_{1i}\right|^{-(1/2)} + \frac{1}{2}\left|e_{1i}\right|^{-1}e_{1i}e_{2i}\right) \\ &\quad + \frac{\lambda_1^2}{2}\left|e_{1i}\right|^{-1}e_{1i}e_{2i} - \frac{\lambda_1}{2}\left|e_{1i}\right|^{-(1/2)}e_{2i}^2 \\ &\quad + \lambda_1\lambda_2\left|e_{1i}\right|^{-(1/2)} + \lambda_1\left|e_{1i}\right|^{-(1/2)}e_{1i}\dot{d}_i \\ &\quad - 2\lambda_2\left|e_{1i}\right|^{-1}e_{1i}e_{2i} - 2e_{2i}\dot{d}_i. \end{aligned} \tag{30}$$

Furthermore, (30) can be written as follows:

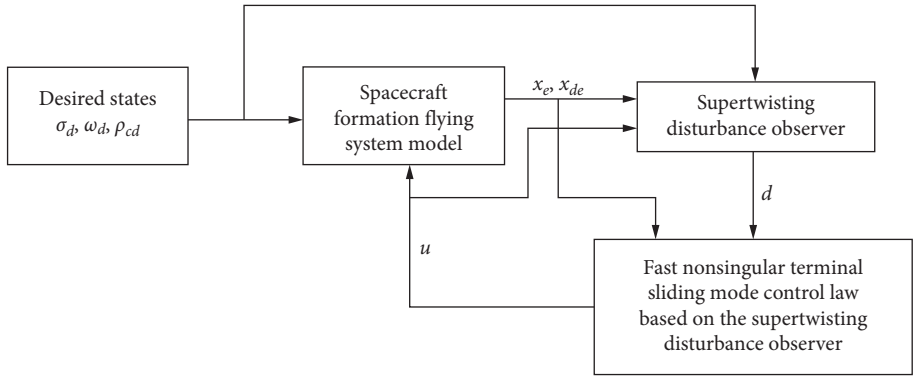

Figure 2: The block diagram of the control law based on the supertwisting disturbance observer.

$$\begin{aligned}\dot{V}_{st} &= -\left(\frac{\lambda_1^3}{2}+\lambda_1\lambda_2\right)\left|e_{1i}\right|^{1/2}+\lambda_1^2 e_{2i}\operatorname{sign}(e_{1i})-\frac{\lambda_1}{2}\frac{e_{2i}^2}{\left|e_{1i}\right|^{1/2}}\\&\quad+\lambda_1\left|e_{1i}\right|^{1/2}\operatorname{sign}(e_{1i})\dot{d}_i-2e_{2i}\dot{d}_i\\&=-\frac{\lambda_1}{2\left|e_{1i}\right|^{1/2}}\left[\left(\lambda_1^2+2\lambda_2\right)\left|e_{1i}\right|-2\lambda_1 e_{2i}\left|e_{1i}\right|^{1/2}\operatorname{sign}(e_{1i})+e_{2i}^2\right]\\&\quad+\frac{\lambda_1}{2\left|e_{1i}\right|^{1/2}}\left[2\left|e_{1i}\right|\operatorname{sign}(e_{1i})-\frac{4}{\lambda_1}\left|e_{1i}\right|^{1/2}e_{2i}\right]\dot{d}_i\\&\le-\frac{\lambda_1}{2\left|e_{1i}\right|^{1/2}}\left[\left(\lambda_1^2+2\lambda_2\right)\left|e_{1i}\right|-2\lambda_1 e_{2i}\left|e_{1i}\right|^{1/2}\operatorname{sign}(e_{1i})+e_{2i}^2\right]\\&\quad+\frac{\lambda_1}{2\left|e_{1i}\right|^{1/2}}\left(2\left|e_{1i}\right|+\frac{4}{\lambda_1}\left|e_{1i}\right|^{1/2}\left|e_{2i}\right|\right)\left|\dot{d}_i\right|.\end{aligned}\tag{31}$$

Since $\kappa_1^2-2|\kappa_1||\kappa_2|+\kappa_2^2\ge 0$, (31) can be rewritten as

$$\begin{aligned}\dot{V}_{st}&\le-\frac{\lambda_1}{2\left|e_{1i}\right|^{1/2}}\left[\left(\lambda_1^2+2\lambda_2\right)\kappa_1^2-2\lambda_1\kappa_1\kappa_2+\kappa_2^2\right]\\&\quad+\frac{\lambda_1}{2\left|e_{1i}\right|^{1/2}}\left(2\kappa_1^2+\frac{4}{\lambda_1}\left|\kappa_1\right|\left|\kappa_2\right|\right)\varsigma_i\\&\le-\frac{\lambda_1}{2\left|e_{1i}\right|^{1/2}}\left[\left(\lambda_1^2+2\lambda_2\right)\kappa_1^2-2\lambda_1\kappa_1\kappa_2+\kappa_2^2\right]\\&\quad+\frac{\lambda_1}{2\left|e_{1i}\right|^{1/2}}\left(2\kappa_1^2+\frac{2}{\lambda_1}\kappa_1^2+\frac{2}{\lambda_1}\kappa_2^2\right)\varsigma_i.\end{aligned}\tag{32}$$

Define the following matrix as

$$\theta_2=\begin{bmatrix}\lambda_1^2+2\lambda_2-\dfrac{2(\lambda_1+1)\varsigma_i}{\lambda_1} & -\lambda_1\\ -\lambda_1 & 1-\dfrac{2\varsigma_i}{\lambda_1}\end{bmatrix}.\tag{33}$$

Then, (32) can be concluded as

$$\dot{V}_{st}\le-\frac{\lambda_1}{2\left|e_{1i}\right|^{1/2}}\kappa^T\theta_2\kappa.\tag{34}$$

From (33), by selecting appropriate observer gains, the matrix θ_2 can be a positive definite matrix. Then, (34) becomes

$$\dot{V}_{st}\le-\frac{\lambda_1\lambda_{\min}(\theta_2)}{2\left|e_{1i}\right|^{1/2}}\|\kappa\|^2,\tag{35}$$

where $\lambda_{\min}(\theta_2)$ is the minimum eigenvalue of θ_2.

θ_1 must to be a positive definite matrix to be Lyapunov matrix; hence, the observer gains λ_1 and λ_2 need to be selected appropriately so that $\theta_1>0$. Let us define the minimal and maximal eigenvalues of θ_1 as $\lambda_{\min}(\theta_1)>0$ and $\lambda_{\max}(\theta_1)>0$, respectively. Then, we have

$$\lambda_{\min}(\theta_1)\|\kappa\|^2\le V_{st}\le\lambda_{\max}(\theta_1)\|\kappa\|^2.\tag{36}$$

Furthermore, by observing from the state vectors κ and κ_1, the following can be concluded:

$$\left|e_{1i}\right|^{1/2}=\sqrt{\kappa_1^2}\le\|\kappa\|.\tag{37}$$

Finally, combining (36) with (37), (35) can be derived as

$$\begin{aligned}&\dot{V}_{st}+\lambda_0 V_{st}^{1/2}\le 0,\\&\lambda_0=\frac{\lambda_1\lambda_{\min}(\theta_1)^{1/2}\lambda_{\min}(\theta_2)}{2\lambda_{\max}(\theta_1)}>0.\end{aligned}\tag{38}$$

Based on (37) and Lemma 1, we prove that $\lim_{t\longrightarrow t_d}e_{1i}=0$ and $\lim_{t\longrightarrow t_d}e_{2i}=0$ with $i=1,2,\ldots,6$. Furthermore, the estimations errors of the state vector x_{1i} and x_{2i} can converge in finite time, and the convergence time is $t_d=2V_{st}^{1/2}/\lambda_0$.

Remark 2. To guarantee that the trajectory errors converge to zero within finite time, the supertwisting disturbance observer gains λ_1 and λ_2 should be selected appropriately so that θ_1 and θ_2 are positive definite matrices.

3.1.2. Fast Nonsingular Terminal Sliding Mode Control Law with Supertwisting Disturbance Observer. To design a fast

nonsingular terminal sliding mode control law, the following sliding mode surface is chosen:

$$s = x_e + \epsilon_1 |x_e|_d^{c_1} \operatorname{sign}(x_e) + \epsilon_2 |x_{de}|_d^{n/m} \operatorname{sign}(x_{de}), \quad (39)$$

where $\epsilon_1, \epsilon_2 > 0$, $c_1 > n/m$, and $1 < n/m < 2$ are all positive constants.

If the spacecraft formation flying system state errors reach the sliding mode $s = 0$, then

$$x_e + \epsilon_1 |x_e|_d^{c_1} \operatorname{sign}(x_e) + \epsilon_2 |x_{de}|_d^{n/m} \operatorname{sign}(x_{de}) = 0. \quad (40)$$

From (15), substituting the equation $\dot{x}_e = x_{de}$ into (40), we have

$$\begin{aligned} \dot{x}_e &= -\left(\frac{1}{\epsilon_2}\right)^{m/n} \left(x_e + \epsilon_1 |x_e|_d^{c_1} \operatorname{sign}(x_e)\right)^{m/n} \\ &= -\left(\frac{1}{\epsilon_2}\right)^{m/n} x_e^{m/n} \left(1 + \epsilon_1 |x_e|_d^{c_1 - 1}\right)^{m/n}. \end{aligned} \quad (41)$$

In order to analyze the fast convergence of the nonsingular fast terminal sliding mode surface, assume that the integration time of the state variable x_e denotes as $x_e(t_i)$ and $x_e(t_i + t_s)$, respectively. Then, integrating the time along both sides of (41),

$$\begin{aligned} \int_{x_e(t_i)}^{x_e(t_i+t_s)} \left(\frac{1}{x_e}\right)^{m/n} \mathrm{d}x_e &= -\int_{t_i}^{t_i+t_s} \left(\frac{1}{\epsilon_2}\right)^{m/n} \left(1 + \epsilon_1 |x_e|^{c_1 - 1}\right)^{m/n} \mathrm{d}\tau \\ &\leq -\int_{t_i}^{t_i+t_s} \left(\frac{1}{\epsilon_2}\right)^{m/n} \mathrm{d}\tau. \end{aligned} \quad (42)$$

Furthermore, it can be seen from (42) that the tracking errors of the spacecraft formation flying system can converge to zero in a limited time $t_s \leq (\epsilon_2^{m/n}/(n-m)) x_e(t_i)^{1-(m/n)}$.

Remark 3. The proposed nonsingular fast terminal sliding mode surface (39) indicates that when the system state variable x_e is far from the equilibrium point, the term x_e plays the major role in making the system trajectory converge at a fast rate. When x_e approaches to the equilibrium point, the term $\epsilon_1 |x_e|_d^{c_1} \operatorname{sign}(x_e)$ plays the dominant role to achieve rapid convergence of the state trajectory.

A design procedure for a fast nonsingular terminal sliding mode control law with a supertwisting disturbance observer is given in the following theorem.

Theorem 1. *Consider the spacecraft formation flying system described by (15) and (16) with*

$$u = C_1^{-1} \left(A x_{de} + g - C_2 \tilde{x}_2\right) - C_1^{-1} M \left(u_0 + u_1 + u_2\right), \quad (43)$$

where

$$u_0 = \frac{1}{\epsilon_2} \frac{m}{n} |x_{de}|_d^{2-(n/m)} \operatorname{sign}(x_{de}), \quad (44)$$

$$u_1 = c_1 \left(\frac{\epsilon_1}{\epsilon_2}\right) \frac{m}{n} |x_{de}|_d^{2-(n/m)} |x_e|_d^{c_1 - 1} \operatorname{sign}(x_{de}), \quad (45)$$

$$u_2 = \alpha_1 \operatorname{sign}(s) + \alpha_2 |s|^{\eta} \operatorname{sign}(s), \quad (46)$$

and $-\alpha_1 sign(s) - \alpha_2 |s|^{\eta} sign(s)$ is the reaching law with $\alpha_1 > 0$, $\alpha_2 > 0$, and $\eta > 1$. Then, the proposed control law along with the supertwisting disturbance observer (26) can guarantee the tracking errors of the spacecraft formation flying system converge to zero in finite time.

Proof. From (39), the derivative of the sliding surface s is given as follows:

$$\begin{aligned} \dot{s} &= \dot{x}_e + \epsilon_1 c_1 |x_e|_d^{c_1 - 1} x_{de} + \epsilon_2 \frac{n}{m} |x_{de}|_d^{(n/m)-1} \dot{x}_{de} \\ &= \dot{x}_e + \epsilon_1 c_1 |x_e|_d^{c_1 - 1} x_{de} + \epsilon_2 \frac{n}{m} |x_{de}|_d^{(n/m)-1} \left(M^{-1} \left(-A x_{de} - g + C_1 u + C_2 d\right)\right). \end{aligned} \quad (47)$$

Consider the following Lyapunov function:

$$V_1(t) = \frac{1}{2} s^{\mathrm{T}} s + \sum_{i=1}^{6} V_{1i}. \quad (48)$$

Taking the time derivative of (48), we have

$$\begin{aligned} \dot{V}_1(t) &= s^{\mathrm{T}} \dot{s} + \sum_{i=1}^{6} \dot{V}_{1i} \\ &= s^{\mathrm{T}} \left(x_{de} + \epsilon_1 c_1 |x_e|_d^{c_1 - 1} x_{de} + \epsilon_2 \frac{n}{m} |x_{de}|_d^{(n/m)-1} \left(-M^{-1} C_2 \cdot \left(x_2 - d\right) - \left(u_0 + u_1 + u_2\right)\right)\right) \\ &\quad - \alpha_0 \sum_{i=1}^{6} V_{1i}^{1/2}. \end{aligned} \quad (49)$$

Substituting the proposed control law (44)–(46) into (49),

$$\begin{aligned} \dot{V}_1(t) &= -s^{\mathrm{T}} \epsilon_2 \frac{n}{m} |x_{de}|_d^{(n/m)-1} \left(\alpha_1 \operatorname{sign}(s) + \alpha_2 |s|^{\eta} \operatorname{sign}(s)\right) \\ &\quad + s^{\mathrm{T}} \epsilon_2 \frac{n}{m} |x_{de}|_d^{(n/m)-1} M^{-1} C_2 \left(x_2 - d\right) \\ &\quad - \alpha_0 \sum_{i=1}^{6} V_{1i}^{1/2}. \end{aligned} \quad (50)$$

Define $x_{de\min} = \min\left\{x_{de1}^{(n/m)-1}, \ldots, x_{de6}^{(n/m)-1}\right\}$, $\overline{\alpha}_1 = x_{de\min} \epsilon_2 (n/m) \alpha_1$, and $\overline{\alpha}_2 = x_{de\min} \epsilon_2 (n/m) \alpha_2$, then

$$\begin{aligned}\dot{V}_1(t) \le & -\overline{\alpha}_1\|s\| - \overline{\alpha}_2\|s\|^{\eta+1} + \epsilon_2\frac{n}{m}s^{\mathrm{T}}\left|x_{de}\right|_d^{(n/m)-1}M^{-1} \\ & C_2(x_2-d) - \alpha_0\sum_{i=1}^{6}V_{1i}^{1/2} \\ \le & -\overline{\alpha}_1\|s\| - \overline{\alpha}_2\|s\|^{\eta+1} + \epsilon_2\frac{n}{m}\|s\|\left\|\left|x_{de}\right|_d^{(n/m)-1}M^{-1}C_2\right\|\|x_2 \\ & -d\| - \alpha_0\sum_{i=1}^{6}V_{1i}^{1/2}.\end{aligned} \tag{51}$$

Define $\alpha_e = \epsilon_2(n/m)\||x_{de}|_d^{(n/m)-1}M^{-1}C_2\|\|x_2 - d\|$ and select $\overline{\alpha}_e = \overline{\alpha}_1 - \alpha_e \ge 0$; we have

$$\dot{V}_1(t) \le -\overline{\alpha}_e\|s\| - \alpha_0\sum_{i=1}^{6}V_{1i}^{1/2}. \tag{52}$$

Finally, define $\alpha_m = \min\{\sqrt{2}\,\overline{\alpha}_e, \alpha_0\}$, then (52) can be rewritten as

$$\begin{aligned}\dot{V}_1(t) &\le -\alpha_m\left(\frac{1}{\sqrt{2}}\|s\| + \sum_{i=1}^{6}V_{1i}^{1/2}\right) \\ &\le -\alpha_m\left(\frac{1}{2}\|s\|^2 + \sum_{i=1}^{6}V_{1i}\right)^{1/2} \\ &= -\alpha_m V_1(t)^{1/2}.\end{aligned} \tag{53}$$

□

Remark 4. When the system state variable is far from the fast nonsingular terminal sliding mode surface, the term $\alpha_2|s|^{\eta}\mathrm{sign}(s)$ in the reaching law plays the major role. On the contrary, the term $\alpha_1\mathrm{sign}(s)$ in the reaching law dominates. By choosing different α_1 and α_2 and selecting appropriate parameters in the fast terminal sliding mode surface, the convergence speed can be controlled. Moreover, compared with the conventional reaching law in [47], the proposed reaching law has faster convergence and better sliding performance. When $s = 0$ and $\dot{s} = 0$, the speed of the state variable approaching the sliding surface is reduced to zero, which can alleviate the chattering phenomenon.

3.2. Fast Nonsingular Terminal Sliding Mode Control Law Based on the Adaptive Neural Network. In this section, an adaptive RBF neural network is employed to approximate the unknown nonlinear A and g in the spacecraft formation flying system (15) and (16), which is not easy to be precisely estimated in practical situations. The block diagram of a fast nonsingular terminal sliding mode control law based on the adaptive neural network is depicted in Figure 3.

The structure of RBF neural network with multiple inputs and multiple outputs is shown in Figure 4.

It can be seen that the RBF neural network has three layers including input layer, output layer, and hidden layer. Denote $x = [x_1, x_2, \ldots, x_n]^{\mathrm{T}}$ as the input, and $\phi_i(x)$ is the Gaussian function of the ith neuron in the hidden layer. Then, the Gaussian function can be expressed as below:

$$\phi_i(x) = \exp\left(-\frac{\|x - c_i\|^2}{2g_i^2}\right), \quad i = 1, 2, \ldots, 6, \tag{54}$$

where c_i is the ith neural radial basis function and g_i is the width of the ith neural radial basis function. In this section, we choose f_{nn} to approximate and compensate the unknown nonlinear parts in the spacecraft formation flying system, where $f_{nn} = -Ax_{de} - g$ is the unknown nonlinear term. We rewrite f_{nn} as follows:

$$f_{nn} = W_i^{\mathrm{T}}\phi_i(x_i) + \xi_i, \tag{55}$$

where W_i denotes the ideal weighting matrix and ξ_i denotes the approximation error, $i = 1, 2, \ldots, 6$.

The estimation of f_{nn} can be expressed as follows:

$$\widehat{f}_{nn} = \widehat{W}_i^{\mathrm{T}}\phi_i(x_i), \tag{56}$$

where $\widehat{W}_i$ denotes the estimation of W_i.

Theorem 2. *Consider the spacecraft formation flying system described by (15) and (16), with the following control law and the adaptive updating law of the RBF neural network:*

$$u = C_1^{-1}\left(\widehat{f}_{nn} - u_3\right) - C_1^{-1}M(u_0 + u_1 + u_2), \tag{57}$$

where

$$u_0 = \frac{1}{\epsilon_2}\frac{m}{n}\left|x_{de}\right|_d^{2-(n/m)}\mathrm{sign}(x_{de}), \tag{58}$$

$$u_1 = c_1\left(\frac{\epsilon_1}{\epsilon_2}\right)\frac{m}{n}\left|x_{de}\right|_d^{2-(n/m)}\left|x_e\right|_d^{c_1-1}\mathrm{sign}(x_{de}), \tag{59}$$

$$u_2 = \alpha_1\mathrm{sign}(s) + \alpha_2|s|^{\eta}\mathrm{sign}(s), \tag{60}$$

$$u_3 = M\left\|M^{-1}C_1\right\|_1\mathrm{sign}(s)d_m, \tag{61}$$

$$\dot{\widehat{W}}_i = \Pi_w\phi_i(x_i)\varrho_i, \tag{62}$$

where ϱ_i is ith element of the term $s^T\epsilon_2(n/m)|x_{de}|_d^{(n/m)-1}M^{-1}$, $i = 1, 2, \ldots, 6$, and Π_w is a positive symmetrical matrix. The tracking errors of the spacecraft formation flying system will converge to zero.

Proof. Define the error of the weighting vector as $\widetilde{W}_i = W_i - \widehat{W}_i$. Consider the following Lyapunov function:

$$V_2(t) = \frac{1}{2}s^{\mathrm{T}}s + \frac{1}{2}\sum_{i=1}^{n}\mathrm{tr}\left(\widetilde{W}_i^T\Pi_w^{-1}\widetilde{W}_i\right). \tag{63}$$

Taking the derivative of (63) with respect to time and substituting the proposed control law (57)–(62) and the adaptive updating law (62), then (63) can be converted as

$$\begin{aligned}\dot{V}_2(t) &= s^{\mathrm{T}}\dot{s} - \sum_{i=1}^{n}\mathrm{tr}\left(\widetilde{W}_i^T\Pi_w^{-1}\dot{\widetilde{W}}_i\right)\\ &= s^{\mathrm{T}}\left(-\epsilon_2\frac{n}{m}|x_{de}|_d^{(n/m)-1}\left(\left\|M^{-1}C_2\right\|_1\mathrm{sign}(s)d_m - M^{-1}C_2d\right)\right)\\ &\quad + \epsilon_2\frac{n}{m}|x_{de}|_d^{(n/m)-1}M^{-1}\widetilde{f}_{nn}\\ &\quad + \epsilon_2\frac{n}{m}|x_{de}|_d^{(n/m)-1}\left(\alpha_1\mathrm{sign}(s) + \alpha_2|s|^{\eta}\mathrm{sign}(s)\right)\\ &\quad - \sum_{i=1}^{n}\mathrm{tr}\left(\widetilde{W}_i^T\Pi_w^{-1}\dot{\widetilde{W}}_i\right).\end{aligned} \tag{64}$$

Since

$$\begin{aligned}&s^T\left(\epsilon_2\frac{n}{m}|x_{de}|_d^{(n/m)-1}\left(-\left\|M^{-1}C_2\right\|_1\mathrm{sign}(s)d_m + M^{-1}C_2d\right)\right)\\ &= -\sum_{i=1}^{6}|s_i|\epsilon_2\frac{n}{m}|x_{de}|_d^{(n/m)-1}\left(M^{-1}C_2\right)\mathrm{sign}(s_i)d_m\\ &\quad + \sum_{i=1}^{6}s_i\epsilon_2\frac{n}{m}|x_{de}|_d^{(n/m)-1}\left(M^{-1}C_2\right)d_i\\ &\le -\sum_{i=1}^{6}|s_i|\epsilon_2\frac{n}{m}|x_{de}|_d^{(n/m)-1}\left|M^{-1}C_2\right|d_m\\ &\quad + \sum_{i=1}^{6}|s_i|\epsilon_2\frac{n}{m}|x_{de}|_d^{(n/m)-1}\left|M^{-1}C_2d_i\right|\\ &\le 0.\end{aligned} \tag{65}$$

Therefore,

$$\begin{aligned}\dot{V}_2(t) &\le s^{\mathrm{T}}\epsilon_2\frac{n}{m}|x_{de}|_d^{(n/m)-1}M^{-1}\widetilde{f}_{nn} + s^{\mathrm{T}}\epsilon_2\frac{n}{m}|x_{de}|_d^{(n/m)-1}\\ &\quad\cdot\left(-\alpha_1\mathrm{sign}(s) - \alpha_2|s|^{\eta}\mathrm{sign}(s)\right)\\ &\quad - \sum_{i=1}^{n}\mathrm{tr}\left(\widetilde{W}_i^T\Pi_w^{-1}\dot{\widetilde{W}}_i\right)\\ &\le s^{\mathrm{T}}\epsilon_2\frac{n}{m}|x_{de}|_d^{(n/m)-1}M^{-1}\sum_{i=1}^{n}\left(\widetilde{W}_i^T\phi_i(x_i) + \xi_i\right)\\ &\quad + s^{\mathrm{T}}\epsilon_2\frac{n}{m}|x_{de}|_d^{(n/m)-1}\left(-\alpha_1\mathrm{sign}(s) - \alpha_2|s|^{\eta}\mathrm{sign}(s)\right)\\ &\quad - \sum_{i=1}^{n}\mathrm{tr}\left(\widetilde{W}_i^T\phi_i(x_i)\right)s^{\mathrm{T}}\epsilon_2\frac{n}{m}|x_{de}|_d^{(n/m)-1}M^{-1}.\end{aligned} \tag{66}$$

Since

$$\begin{aligned}&s^{\mathrm{T}}\epsilon_2\frac{n}{m}|x_{de}|_d^{(n/m)-1}M^{-1}\sum_{i=1}^{n}\left(\widetilde{W}_i^{\mathrm{T}}\phi_i(x_i)\right)\\ &= -\sum_{i=1}^{n}\mathrm{tr}\left(\widetilde{W}_i^{\mathrm{T}}\phi_i(x_i)\right)s^{\mathrm{T}}\epsilon_2\frac{n}{m}|x_{de}|_d^{(n/m)-1}M^{-1},\end{aligned} \tag{67}$$

(66) can be rewritten as follows:

$$\begin{aligned}\dot{V}_2(t) &\le -s^{\mathrm{T}}\epsilon_2\frac{n}{m}|x_{de}|_d^{(n/m)-1}\left(\alpha_1\mathrm{sign}(s) + \alpha_2|s|^{\eta}\mathrm{sign}(s)\right)\\ &\quad + \epsilon_2\frac{n}{m}|x_{de}|_d^{(n/m)-1}s^{\mathrm{T}}M^{-1}\sum_{i=1}^{n}\xi_i\\ &\le -\overline{\alpha}_1\|s\| - \overline{\alpha}_2\|s\|^{\eta+1} + \epsilon_2\frac{n}{m}s^{\mathrm{T}}|x_{de}|_d^{(n/m)-1}\\ &\quad\cdot|x_{de}|_d^{(n/m)-1}M^{-1}\sum_{i=1}^{n}\xi_i\\ &\le -\overline{\alpha}_1\|s\| - \overline{\alpha}_2\|s\|^{\eta+1} + \epsilon_2\frac{n}{m}\|s\|\\ &\quad\cdot\left\||x_{de}|_d^{n/m(n/m)-1-1}M^{-1}\sum_{i=1}^{n}\xi_i\right\|.\end{aligned} \tag{68}$$

Define $\xi_h = \epsilon_2(n/m)\||x_{de}|_d^{(n/m)-1}M^{-1}\sum_{i=1}^{n}\xi_i\|$, then we have

$$\dot{V}_2(t) \le -\overline{\xi}\|s\|, \tag{69}$$

where $\overline{\xi} = \overline{\alpha}_1 - \xi_h$.

Therefore, it can be concluded that the tracking errors of the spacecraft formation flying system converge to zero and the proof is completed. □

4. Numerical Simulation

In this section, the simulation result that shows the effectiveness of the supertwisting disturbance observer, the nonsingular fast terminal sliding mode control law, and the adaptive neurosliding mode control law are presented, respectively, in each section.

The parameters in the formation flying system are given as follows: the masses of the target and the chaser spacecraft are $m_t = m_c = 110\,\mathrm{kg}$, the initial orbit parameters of the target spacecraft are set as the semimajor axis $a = 7000\,\mathrm{km}$, the eccentricity $e = 0.01$, the orbit inclination $i = 30^{\circ}$, and the ascending node is $\Omega = 45^{\circ}$, and apogee and perigee are both 0°.

The inertial matrix of the chaser spacecraft is $J = [3\ 1\ 0.7; 1\ 3.5\ 1; 0.5\ 1\ 4]\,\mathrm{kg\cdot m^2}$, and the disturbance torque $d_\tau = 0.1[\sin(t)\ -\cos(0.3t)\sin(0.5t)]^{\mathrm{T}}\,\mathrm{Nm}$. The desired attitude and position are given as $\rho_{cd} = [2\ -2\ -0.5]^{\mathrm{T}}m$ and $\sigma_d = 0.001[\sin(10t)\ -\cos(10t)\sin(10t)]^{\mathrm{T}}$.

4.1. Supertwisting Disturbance Observer. The gains of the supertwisting disturbance observer are chosen as $\lambda_1 = 2$ and

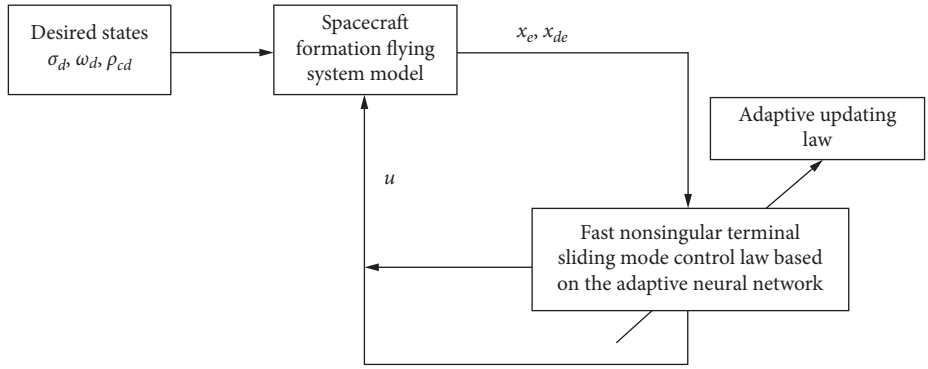

Figure 3: The block diagram of the control law based on the adaptive neural network.

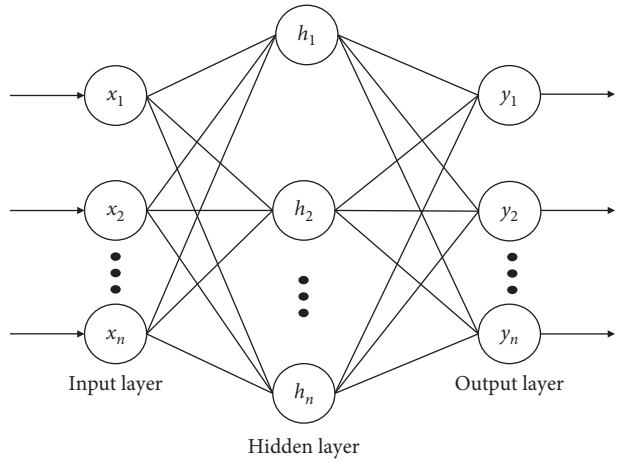

Figure 4: The structure of RBF neural network.

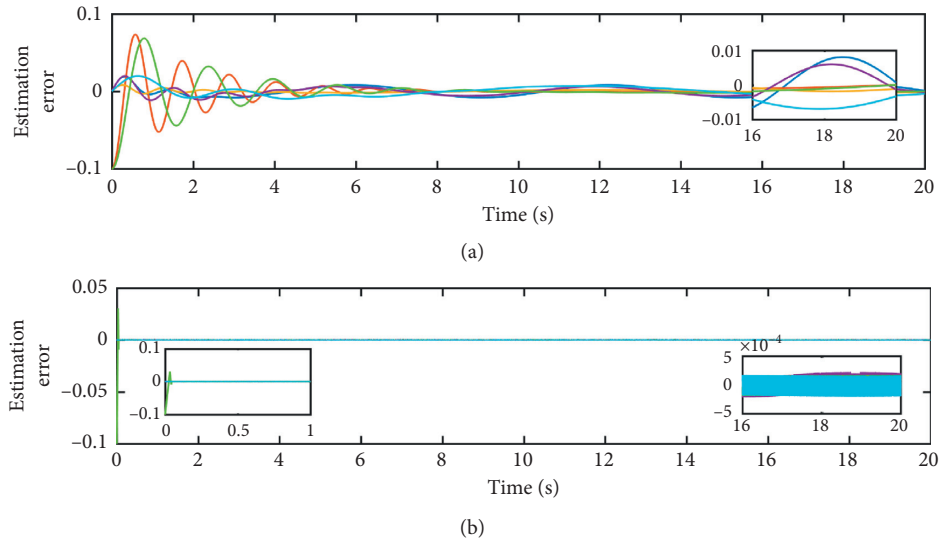

Figure 5: Comparisons of disturbance estimation error between (a) the linear disturbance observer and (b) the supertwisting disturbance observer.

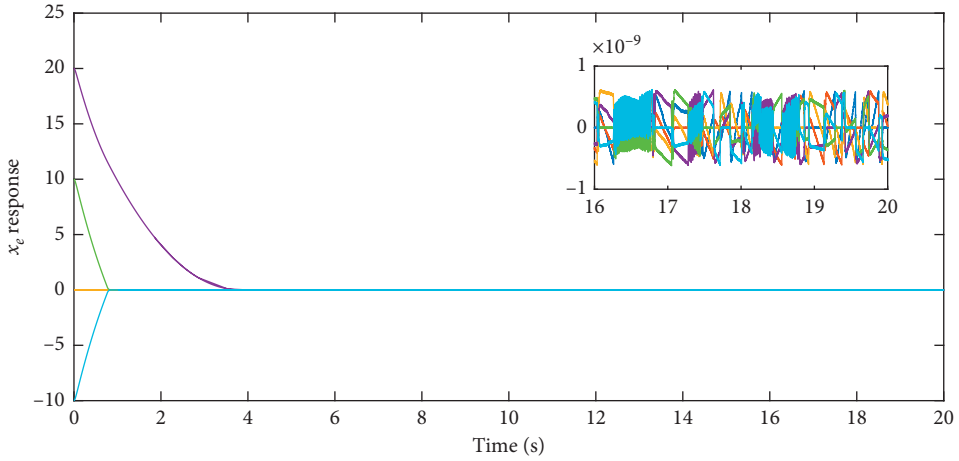

Figure 6: The state responses of x_e with the fast nonsingular terminal sliding mode control law (43) based on the supertwisting disturbance observer.

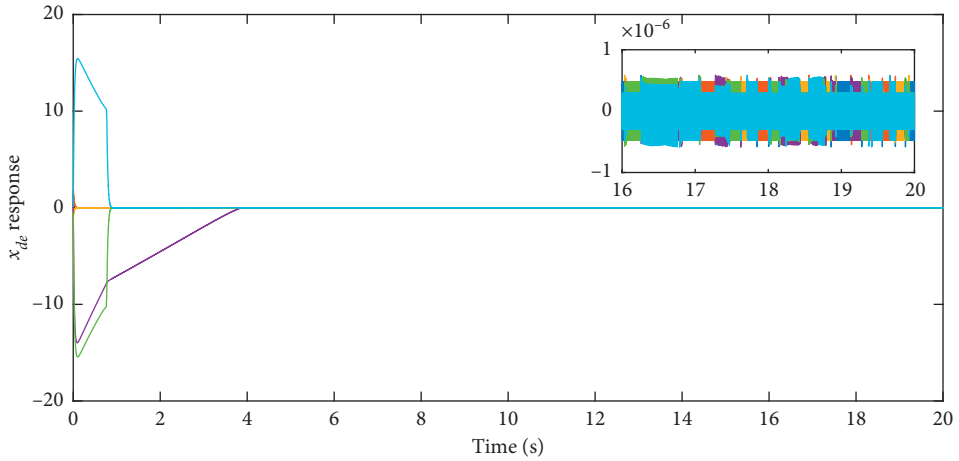

Figure 7: The state responses of x_{de} with the fast nonsingular terminal sliding mode control law (43) based on the supertwisting disturbance observer.

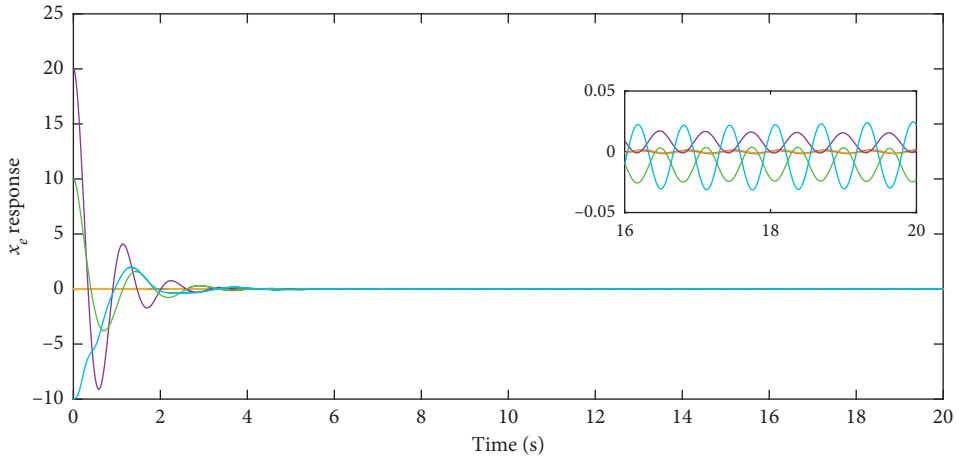

Figure 8: The state responses of x_e with the nonlinear PD control law (72).

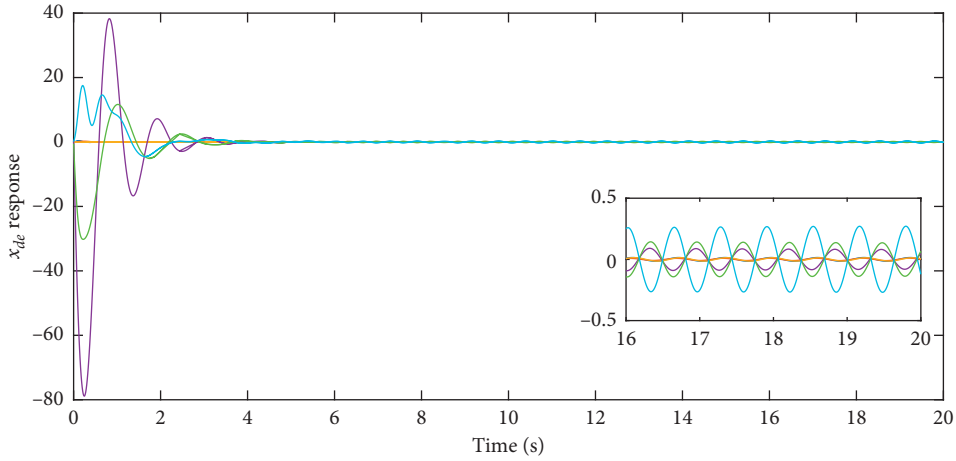

Figure 9: The state responses of x_{de} with the nonlinear PD control law (72).

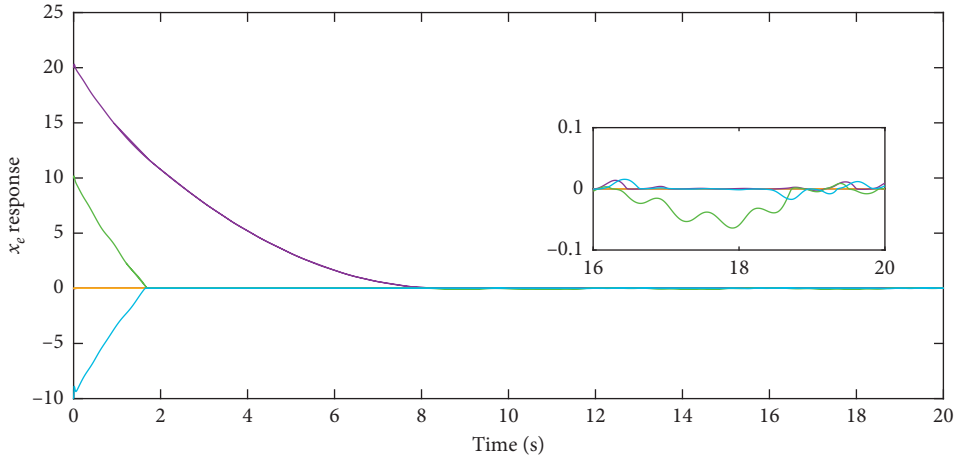

Figure 10: The state responses of x_e with the fast nonsingular terminal sliding mode control law (57) based on the adaptive RBF neural network.

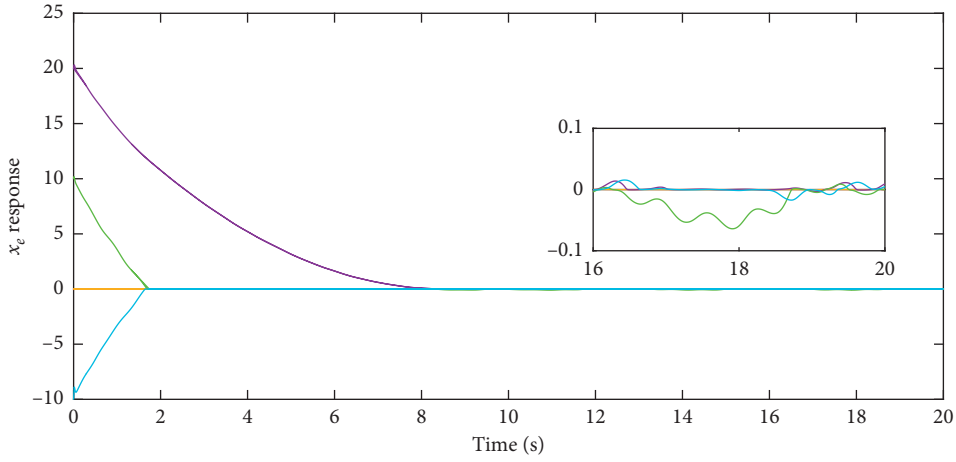

Figure 11: The state responses of x_{de} with the fast nonsingular terminal sliding mode control law (57) based on the adaptive RBF neural network.

$\lambda_2 = 4$. In order to demonstrate the advantage of the proposed supertwisting disturbance observer, we compare its performance with the traditional linear observer as below:

$$\begin{cases} \dot{\hat{x}}_1 = -L_1(x_1 - \hat{x}_1) + x_2, \\ \dot{\hat{x}}_2 = -L_2(x_2 - \hat{x}_2). \end{cases} \tag{70}$$

The L_1 and L_2 in (70) are selected as

$$L_1 = \text{diag}\{0.023, 0.011, 0.014, 0.012, 0.010, 0.008\} \times 10^4,$$
$$L_2 = \text{diag}\{1.320, 0.300, 0.400, 0.270, 0.160, 0.070\} \times 10^4. \tag{71}$$

The disturbance estimation error given by the linear disturbance observer (70) and the proposed supertwisting disturbance observer (26) are depicted in Figures 5(a) and 5(b), respectively.

Remark 5. It can be seen from Figure 5 that the supertwisting disturbance observer estimation error converges to zero in finite time, whereas the estimation error from the linear disturbance observer takes longer time to converge to zero. Therefore, the proposed supertwisting observer can estimate the disturbance in finite time, which demonstrates its advantage over the linear one in the spacecraft formation flying system.

4.2. The Nonsingular Fast Terminal Sliding Mode Control Law with Supertwisting Disturbance Observer. The parameters for the nonsingular fast terminal sliding mode surface are set as $\epsilon_1 = 0.1$, $\epsilon_2 = 0.02$, $c_1 = 27/19$, and $n/m = 21/19$. The parameters in the control law are set as $\alpha_1 = 100$, $\alpha_2 = 0.1$, $\epsilon = 0.5$, and $\eta = 1.5$.

The state responses of x_e and x_{de} under the proposed control sliding model control law (43) are given in Figures 6 and 7, respectively.

Furthermore, to illustrate the effectiveness of the proposed control law, in this part, we compare it with a widely used nonlinear PD control law given as follows:

$$u = C_1^{-1} M\left(-K_p x_e - K_d x_{de}\right), \tag{72}$$

where the coefficient K_p and K_d are calculated as follows:

$$K_p = \text{diag}\{16.5, 3.75, 50, 13.5, 20, 8.75\},$$
$$K_d = \text{diag}\{5.75, 2.75, 3.5, 3.0, 2.5, 2.0\}. \tag{73}$$

The state responses of vectors x_e and x_{de} under the nonlinear PD control law are given in Figures 8 and 9.

Remark 6. From Figures 6–9, it can be seen that the proposed control law (43) yields better transient responses as compared to the nonlinear PD control law. Also, it is obvious that the proposed control law (43) guarantees the tracking errors converge to zero in a finite time.

4.3. Adaptive Neurosliding Mode Control Law. The parameters of the RBF neural network, c_i is evenly selected over the space and $g_i = 10$. 200 neurons are used to approximate each f_{nm_i}. $\Pi_w = \text{diag}\{100, 100, 100, 100, 100, 100, 100\}$.

The state responses of the system under the RBF neural network control law (57) are given in Figures 10 and 11.

Remark 7. Figures 10 and 11 indicate that the tracking errors converge to a small region of zero with a good adaptive performance. This concludes that the RBF neural network control law (57) is able to compensate for the unknown dynamics in the spacecraft formation flying system.

5. Conclusion

This paper has proposed the nonsingular fast terminal sliding mode control laws to solve the tracking control problem for spacecraft formation flying systems. First, a supertwisting disturbance observer has been introduced to estimate the disturbances in finite time. Then, based on a nonsingular fast terminal sliding mode surface, a novel control law has been presented to guarantee the tracking errors of the spacecraft formation converge to zero in finite time. Furthermore, for the unknown nonlinear parts in the spacecraft formation flying system, a RBF neural network has been proposed to approximate them and then compensate them. Finally, via simulations the effectiveness of the proposed control laws has been demonstrated. In our future work, we will investigate (1) the spacecraft formation system subject to the time-delay on terminal adaptive neurosliding mode control [48, 49] and (2) nonlinear observer design for the spacecraft formation system.

Data Availability

The data used to support the findings of this study are available from the corresponding author upon request.

Conflicts of Interest

All authors declare that they have no conflicts of interest.

Acknowledgments

This work was supported by the Scholarship from China Scholarship Council.

References

[1] K. Lu, Y. Xia, and M. Fu, "Controller design for rigid spacecraft attitude tracking with actuator saturation," *Information Sciences*, vol. 220, pp. 343–366, 2013.

[2] L. Sun, W. Huo, and Z. Jiao, "Adaptive backstepping control of spacecraft rendezvous and proximity operations with input saturation and full-state constraint," *IEEE Transactions on Industrial Electronics*, vol. 64, no. 1, pp. 480–492, 2017.

[3] H.-T. Chen, S.-M. Song, and Z.-B. Zhu, "Robust finite-time attitude tracking control of rigid spacecraft under actuator saturation," *International Journal of Control, Automation and Systems*, vol. 16, no. 1, pp. 1–15, 2018.

[4] Q. Li, B. Zhang, J. Yuan, and H. Wang, "Potential function based robust safety control for spacecraft rendezvous and

proximity operations under path constraint," *Advances in Space Research*, vol. 62, no. 9, pp. 2586–2598, 2018.

[5] Z. Zhu, Y. Guo, and Z. Gao, "Adaptive finite-time actuator fault-tolerant coordinated attitude control of multispacecraft with input saturation," *International Journal of Adaptive Control and Signal Processing*, vol. 33, no. 4, pp. 644–663, 2019.

[6] M.-D. Tran and H.-J. Kang, "Nonsingular terminal sliding mode control of uncertain second-order nonlinear systems," *Mathematical Problems in Engineering*, vol. 2015, Article ID 181737, 8 pages, 2015.

[7] J. Wan, T. Hayat, and F. E. Alsaadi, "Adaptive neural globally asymptotic tracking control for a class of uncertain nonlinear systems," *IEEE Access*, vol. 7, pp. 19054–19062, 2019.

[8] E. Capello, E. Punta, F. Dabbene, G. Guglieri, and R. Tempo, "Sliding-mode control strategies for rendezvous and docking maneuvers," *Journal of Guidance, Control, and Dynamics*, vol. 40, no. 6, pp. 1481–1487, 2017.

[9] C. Pukdeboon, "Adaptive backstepping finite-time sliding mode control of spacecraft attitude tracking," *Journal of Systems Engineering and Electronics*, vol. 26, pp. 826–839, 2015.

[10] B. Cai, L. Zhang, and Y. Shi, "Control synthesis of hidden semi-markov uncertain fuzzy systems via observations of hidden modes," *IEEE Transactions on Cybernetics*, pp. 1–10, 2019.

[11] X. Lin, X. Shi, and S. Li, "Optimal cooperative control for formation flying spacecraft with collision avoidance," *Science Progress*, vol. 103, no. 1, pp. 1–9, 2020.

[12] R. Liu, M. Liu, and Y. Liu, "Nonlinear optimal tracking control of spacecraft formation flying with collision avoidance," *Transactions of the Institute of Measurement and Control*, vol. 41, no. 4, pp. 889–899, 2019.

[13] X. Cao, P. Shi, Z. Li, and M. Liu, "Neural-network-based adaptive backstepping control with application to spacecraft attitude regulation," *IEEE Transactions on Neural Networks and Learning Systems*, vol. 29, no. 9, pp. 4303–4313, 2018.

[14] Y. Wang, B. Jiang, Z.-G. Wu, S. Xie, and Y. Peng, "Adaptive sliding mode fault-tolerant fuzzy tracking control with application to unmanned marine vehicles," *IEEE Transactions on Systems, Man, and Cybernetics: Systems*, pp. 1–10, 2020.

[15] J. Fei and Z. Feng, "Adaptive fuzzy super-twisting sliding mode control for microgyroscope," *Complexity*, vol. 2019, Article ID 6942642, 13 pages, 2019.

[16] J. Fei and H. Wang, "Experimental investigation of recurrent neural network fractional-order sliding mode control for active power filter," *IEEE Transactions on Circuits and Systems II-Express Briefs*, 2019.

[17] Y. Wang, W. Zhou, J. Luo, H. Yan, H. Pu, and Y. Peng, "Reliable intelligent path following control for a robotic airship against sensor faults," *IEEE/ASME Transactions on Mechatronics*, vol. 24, no. 6, pp. 2572–2582, 2019.

[18] G.-Q. Wu and S.-M. Song, "Antisaturation attitude and orbit-coupled control for spacecraft final safe approach based on fast nonsingular terminal sliding mode," *Journal of Aerospace Engineering*, vol. 32, no. 2, 2019.

[19] D. Ran, B. Xiao, T. Sheng, and X. Chen, "Adaptive finite time control for spacecraft attitude maneuver based on second-order terminal sliding mode," *Proceedings of the Institution of Mechanical Engineers, Part G: Journal of Aerospace Engineering*, vol. 231, no. 8, pp. 1415–1427, 2017.

[20] Z. Wang, Y. Su, and L. Zhang, "A new nonsingular terminal sliding mode control for rigid spacecraft attitude tracking," *Journal Dynamic System, Measurement, Control*, vol. 140, no. 5, 2018.

[21] C. Jing, H. Xu, X. Niu, and X. Song, "Adaptive nonsingular terminal sliding mode control for attitude tracking of spacecraft with actuator faults," *IEEE Access*, vol. 7, pp. 31485–31493, 2019.

[22] L. Yang and Y. Jia, "Finite-time attitude tracking control for a rigid spacecraft using time-varying terminal sliding mode techniques," *International Journal of Control*, vol. 88, no. 6, pp. 1150–1162, 2015.

[23] J. Fei and Z. Feng, "Fractional-order finite-time super-twisting sliding mode control of micro gyroscope based on double-loop fuzzy neural network," *IEEE Transactions on Systems, Man, and Cybernetics: Systems*, pp. 1–15, 2020.

[24] L. Tao, Q. Chen, and Y. Nan, "Disturbance-observer based adaptive control for second-order nonlinear systems using chattering-free reaching law," *International Journal of Control, Automation and Systems*, vol. 17, no. 2, pp. 356–369, 2019.

[25] L. Zhou, J. She, S. Zhou, and C. Li, "Compensation for state-dependent nonlinearity in a modified repetitive control system," *International Journal of Robust and Nonlinear Control*, vol. 28, no. 1, pp. 213–226, 2018.

[26] Q. Li, J. Yuan, B. Zhang, and H. Wang, "Disturbance observer based control for spacecraft proximity operations with path constraint," *Aerospace Science and Technology*, vol. 79, pp. 154–163, 2018.

[27] W. Deng and J. Yao, "Extended-state-observer-based adaptive control of electro-hydraulic servomechanisms without velocity measurement," *IEEE/ASME Transactions on Mechatronics*, p. 1, 2019.

[28] W. Deng, J. Yao, and D. Ma, "Time-varying input delay compensation for nonlinear systems with additive disturbance: an output feedback approach," *International Journal of Robust and Nonlinear Control*, vol. 28, no. 1, pp. 31–52, 2018.

[29] A. A. Godbole, J. P. Kolhe, and S. E. Talole, "Performance analysis of generalized extended state observer in tackling sinusoidal disturbances," *IEEE Transactions on Control Systems Technology*, vol. 21, no. 6, pp. 2212–2223, 2013.

[30] Q. Zong, Q. Dong, F. Wang, and B. Tian, "Super twisting sliding mode control for a flexible air-breathing hypersonic vehicle based on disturbance observer," *Science China Information Sciences*, vol. 58, no. 7, pp. 1–15, 2015.

[31] H. Yoon, Y. Eun, and C. Park, "Adaptive tracking control of spacecraft relative motion with mass and thruster uncertainties," *Aerospace Science and Technology*, vol. 34, pp. 75–83, 2014.

[32] A.-M. Zou, K. D. Kumar, and Z.-G. Hou, "Distributed consensus control for multi-agent systems using terminal sliding mode and Chebyshev neural networks," *International Journal of Robust and Nonlinear Control*, vol. 23, no. 3, pp. 334–357, 2013.

[33] M. Van and H.-J. Kang, "Robust fault-tolerant control for uncertain robot manipulators based on adaptive quasi-continuous high-order sliding mode and neural network," *Proceedings of the Institution of Mechanical Engineers, Part C: Journal of Mechanical Engineering Science*, vol. 229, no. 8, pp. 1425–1446, 2015.

[34] Y. Sun, G. Ma, L. Chen, and P. Wang, "Neural network-based distributed adaptive configuration containment control for satellite formations," *Proceedings of the Institution of Mechanical Engineers, Part G: Journal of Aerospace Engineering*, vol. 232, no. 12, pp. 2349–2363, 2017.

[35] Y. Sun, L. Chen, G. Ma, and C. Li, "Adaptive neural network tracking control for multiple uncertain Euler-Lagrange systems with communication delays," *Journal of the Franklin Institute*, vol. 354, no. 7, pp. 2677–2698, 2017.

[36] Z. Jin, J. Chen, Y. Sheng, and X. Liu, "Neural network based adaptive fuzzy PID-type sliding mode attitude control for a reentry vehicle," *International Journal of Control, Automation and Systems*, vol. 15, no. 1, pp. 404–415, 2017.

[37] C. Yang, T. Teng, B. Xu, Z. Li, J. Na, and C.-Y. Su, "Global adaptive tracking control of robot manipulators using neural networks with finite-time learning convergence," *International Journal of Control, Automation and Systems*, vol. 15, no. 4, pp. 1916–1924, 2017.

[38] L. Zhao and Y. Jia, "Neural network-based distributed adaptive attitude synchronization control of spacecraft formation under modified fast terminal sliding mode," *Neurocomputing*, vol. 171, pp. 230–241, 2016.

[39] D. Sun, F. Naghdy, and H. Du, "Neural network-based passivity control of teleoperation system under time-varying delays," *IEEE Transactions on Cybernetics*, vol. 47, no. 7, pp. 1666–1680, 2017.

[40] N. Zhou, R. Chen, Y. Xia, and J. Huang, "Estimator-based adaptive neural network control of leader-follower high-order nonlinear multiagent systems with actuator faults," *Concurrency and Computation: Practice and Experience*, vol. 29, no. 24, pp. 1–13, 2017.

[41] X. Gao, X. Zhong, D. You, and S. Katayama, "Kalman filtering compensated by radial basis function neural network for seam tracking of laser welding," *IEEE Transactions on Control Systems Technology*, vol. 21, no. 5, pp. 1916–1923, 2013.

[42] J. Fei and Y. Chen, "Dynamic terminal sliding mode control for single-phase active power filter using double hidden layer recurrent neural network," *IEEE Transactions on Power Electronics*, vol. 35, no. 9, pp. 9906–9924, 2020.

[43] Y. Hong, J. Wang, and D. Cheng, "Adaptive finite-time control of nonlinear systems with parametric uncertainty," *IEEE Transactions on Automatic Control*, vol. 51, no. 5, pp. 858–862, 2006.

[44] C. Pukdeboon, "Output feedback second order sliding mode control for spacecraft attitude and translation motion," *International Journal of Control, Automation and Systems*, vol. 14, no. 2, pp. 411–424, 2016.

[45] T. Chen and H. Chen, "Approximation capability to functions of several variables, nonlinear functionals, and operators by radial basis function neural networks," *IEEE Transactions Neural Network*, vol. 6, no. 4, pp. 904–910, 1995.

[46] E. Duraffourg, L. Burlion, and T. Ahmed-Ali, "Finite-time observer-based backstepping control of a flexible launch vehicle," *Journal of Vibration and Control*, vol. 24, no. 8, pp. 1535–1550, 2018.

[47] N. Tino, P. Siricharuanun, and C. Pukdeboon, "Chaos synchronization of two different chaotic systems via nonsingular terminal sliding mode techniques," *Thai Journal of Mathematics*, vol. 14, pp. 22–36, 2016.

[48] X. Ge, Q.-L. Han, and X.-M. Zhang, "Achieving cluster formation of multi-agent systems under aperiodic sampling and communication delays," *IEEE Transactions on Industrial Electronics*, vol. 65, no. 4, pp. 3417–3426, 2018.

[49] B.-L. Zhang, Q.-L. Han, X.-M. Zhang, and X. Yu, "Sliding mode control with mixed current and delayed states for offshore steel jacket platforms," *IEEE Transactions on Control Systems Technology*, vol. 22, pp. 1769–1783, 2014.